Polymer 181 (2019) 121765

Contents lists available at ScienceDirect

Polymer

journal homepage: www.elsevier.com/locate/polymer

The effects of staged mixing on the dispersion of reinforcing fillers in elastomer compounds

Alex McGlasson[a], Kabir Rishi[a], Gregory Beaucage[a,*], Vishak Narayanan[a], Michael Chauby[a], Andrew Mulderig[a], Vikram K. Kuppa[b], Jan Ilavsky[c], Mindaugas Rackaitis[d]

[a] University of Cincinnati, Cincinnati, OH, 45221-0012, United States
[b] Nonstructural Materials Division, University of Dayton Research Institute, Dayton, OH, 45469, United States
[c] Advanced Photon Source, Argonne National Laboratory, Argonne, IL, United States
[d] Bridgestone Americas Center for Research and Technology, Akron, OH, 44301, United States

HIGHLIGHTS

- Nano-scale dispersion of filler quantified by small-angle X-ray scattering.
- Colloidal analogy relates thermal motion to kinetic dispersion via accumulated strain.
- Filler interactions modelled by two parameters from the van der Waals equation.
- Aggregate excluded volume related to the hard-sphere aggregate volume.
- Aggregate interaction energy depends on the extent of carbon coverage on the silica surface.

ARTICLE INFO

Keywords:
Nanocomposite
Ultra small-angle X-ray scattering
Kinetic dispersion
Colloidal model
van der Waals
Excluded volume
Accumulated strain
Carbon coverage on silica surface

ABSTRACT

Kinetically mixed reinforcing fillers are dispersed by accumulated strain. Processing conditions such as mixing geometry, intensity and the duration of mixing are key elements that control accumulated strain. A simple method to modify mechanical mixing is the mixing schedule which involves the timing of filler additions to a compound. For example, it is known that simultaneous addition of oil with filler is disadvantageous to dispersion, while the incorporation of oil after filler addition enhances dispersion. The simplest case of mixing schedule involves timed filler additions into an elastomer, for instance in a single stage or in two-stages. This study explores the effects of staged mixing on nanoscale dispersion based on a colloidal model. Dispersion is quantified using a pseudo-thermodynamic approach coupled with ultra-small angle X-ray scattering. It was found that single stage mixing yields optimal nano-dispersion for carbon-coated silica and carbon black in polybutadiene using an internal mixer.

1. Introduction

Compounding of an elastomer and filler is a complicated process that involves multiple steps such as wetting of the filler by the elastomer, breakup of filler agglomerates into aggregates of small size, and dispersion of these aggregates. Each step is characterized by different parameters, for example, filler incorporation time or wetting time is generally determined from the power peak in the torque curves [1]. The dispersive mixing step is characterized by assigning a dispersion rating based on reduction in micron-scale agglomerate size during the mixing process [2–4]. Similarly, aggregate distribution is characterized through a statistically determined mixing index [5,6]. All of these metrics pertain to the micron scale. Reinforcing fillers are generally immiscible in the elastomer matrix meaning that an equilibrium colloidal dispersion cannot be reached and dispersion is maintained by kinetically locking-in a mechanically generated non-equilibrium state. This leads to local clustering of particles on the nanoscale and dispersion of larger agglomerates of these nano-clusters at larger scales creating a hierarchical network [7]. The combined breakup and distribution of filler particles depends on particle morphology, accumulated strain as a function of residence time, and the mixer geometry which govern the total strain imparted to the elastomer compound. Thus, the total accumulated shear strain and the proportional residence time in the mixer at a constant shear rate are related directly to filler

* Corresponding author.
E-mail address: gbeaucage@gmail.com (G. Beaucage).

https://doi.org/10.1016/j.polymer.2019.121765
Received 22 May 2019; Received in revised form 26 August 2019; Accepted 30 August 2019
Available online 30 August 2019

dispersion [8]. Throughout this article, the dispersion process refers to a combination of the four main steps: wetting of the filler, breakup of agglomerates, dispersion and clustering of aggregates and formation of a micron-scale network of clusters. The dispersion process is controlled by material properties such as viscosity and filler structure and processing variables such as mixing time, mixer geometry and type. Given the importance of the processing variables, sequential mixing of a fraction of the filler could have some advantage [9,10]. In the tire industry, a widespread practice is to break up filler additions into stages so that all the filler is not added at one time. It is commonly believed that if the filler is added all at once, clustering of filler could lead to an uneven distribution in the matrix. In the interest of understanding this empirical assumption, quantitative measurement of the nano-dispersion of reinforcing filler in elastomers is examined in this paper.

Estimation of the degree of dispersion is largely based on the physical and mechanical properties as well as the bound rubber content of the filled elastomers [9,10]. It is generally accepted that an improvement in properties under different processing conditions indicates better dispersion. However, quantification of filler dispersion relies on microscopy, rheology, and other techniques such as electrical conductivity [11–14]. Coran et al. used optical dark field microscopy and compared their micrographs against a standard [2]. The extent of filler dispersion was quantified by assigning a dispersion rating modelled on the fraction of undispersed filler agglomerates. Feke et al. proposed a model for reduction in agglomerate size based on the competition of hydrodynamic forces in the mixer and the cohesive forces holding the aggregates within an agglomerate together [4]. This model was compared to the dispersion rating determined by Coran et al. In either case, the dispersion rating was found to improve with processing parameters such as mixing time. Since the rating is assigned based on a set of standard micrographs, the extent of filler aggregate distribution at the culmination of processing is largely empirical. However, the mixing index proposed by Kalyon et al. could be a suitable measure of aggregate distribution [5]. The mixing index was based on the ratio of the standard deviation in aggregate concentration in the mix to the standard deviation of a completely segregated filler. The standard deviations in filler concentrations were obtained by conducting thermogravimetric analysis on different specimens [15]. The standard deviations in filler concentration have also been determined by the intensity ratio of distinct phases in wide-angle X-ray diffraction [15,16]. However, this statistical technique relies on sampling a large data set to get an accurate measure of variances. Although the distributive mixing index correlates well to the electrical conductivity, [5] this technique seems to be a qualitative measure of filler dispersion rather than quantitative, as noted by Rueda et al. [6] These methods measure dispersion on the macro scale. The size scale is on the order of millimeters for TGA measurements and on the order of microns for XRD.

A new colloidal approach to quantify nanoscale dispersion for reinforced elastomers involving X-ray scattering can describe dispersion based on an analogy between thermally dispersed colloids and kinetically dispersed filler particles [17–19]. The terminology of polymer solutions is adopted so that low concentrations where isolated nanoparticle aggregates exist are termed dilute. A semi-dilute solution is defined when aggregates significantly interact. This would occur at an overlap concentration $\phi_V{}^*$, when a loss in normalized scattering intensity is observed as discussed below. Concentrated conditions are generally not observed under normal elastomer reinforcement conditions. The colloidal model is based on the observation that the normalized scattered intensity, $I(q)/\phi_V$, at intermediate scattering vector, q decays with concentration for semi-dilute filled elastomers in a way that parallels the decay with structural screening for thermally dispersed colloids [17–19]. The rate of decay with concentration is a measure of the innate dispersibility of an elastomer compound. As opposed to colloidal dispersions, for the case of reinforced elastomers, the dispersion is driven by mechanical mixing rather than thermal motion. Borrowing from protein and polymer solutions, this decay in normalized scattered intensity can measure the pseudo-second order virial coefficient, A_2, which is related to the quality of the dispersion. For negative values of A_2 the system phase separates. However, a more positive value of A_2 indicates better filler dispersion. $A_2 = 0$ defines a critical point where the filler de-mixes.

On a nanoscale the second virial coefficient can be measured using small angle X-ray scattering (SAXS) using a concentration series where a dilute sample of about 1 wt% filler is first measured. This dilute scattering curve is fit using the Unified Scattering Function, [20–22].

$$I_0(q) = \sum_{i=0}^{2} \left\{ G_i exp\left(-q^2 R_{g,i}{}^2 / 3 \right) + B_i (q_i^*)^{-P_i} exp\left(-q^2 R_{g,i+1}{}^2 / 3 \right) \right\} \quad (1)$$

$$q_i^* = q / \left(erf\{1.06 q R_{g,i} / \sqrt{6}\} \right)^3 \quad (2)$$

where, 'i' indicates the structural level. G_i and B_i are the Guinier and Porod pre-factors respectively, $R_{g,i}$ is the radius of gyration and a measure of the feature size at each structural level, whereas P_i is the power-law exponent that indicates the morphology of the feature. The scattering vector, q, is inversely related to the spatial distance. That is, small structural levels are observed at high q. In equation (2), *erf* is the error function. Reinforcing fillers such as silica and carbon black are made of various structural levels at distinct size scales. The largest structural level for these fillers is that of an agglomerate with a size in the range of a few microns. Commercial filler particles/powders exist as micron to millimeter size agglomerates. Since the dispersion process leads to reduction in the size of these agglomerates, the structural levels important to nano-dispersion are that of the aggregate (level 2) and the primary particle (level 1). The primary particles fuse together to form filler aggregates. The aggregates themselves are also held together by van der Waals forces to form large agglomerates. The energy supplied in an internal mixer is sufficient to overcome the weak van der Waals forces but not strong enough to breakup aggregates. Consequently, the colloidal model focuses on aggregate dispersion in the filler matrix.

Structural screening at high filler concentrations ϕ_V, manifests as a loss in normalized scattered intensity. This is quantified using the random phase approximation, [19,23].

$$\left(I(q, \phi_V) / \phi_V \right)^{-1} = \left(I_0(q, \phi_{V,0}) / \phi_{V,0} \right)^{-1} + \nu \phi_V \quad (3)$$

where, ϕ_V is the volume fraction of filler in the compound and ν is a measure of the extent of structural screening. The greater the dispersion the greater the degree of structural screening. $1/\nu\phi_v$ is the low-q plateau value of normalized intensity which varies with filler concentration. The subscript "0" in equation (3) refers to dilute concentration, $\phi_{V,0}$ of the fractal aggregates where structural screening does not impact the observed normalized intensity. The structural screening parameter ν, is unique for each filler-elastomer and processing combination and is related to the pseudo-second virial coefficient, A_2 as [17].

$$A_2 = \nu \Delta\rho^2 / 2 N_A \rho^2 \quad (4)$$

Where, $\Delta\rho^2$ is the square of the difference in scattering length densities of the filler and elastomer, also known as the contrast, N_A is the Avogadro's number and ρ is the density of the filler, ~1.9 g cm^{-3} for carbon black and ~2.2 g cm^{-3} for silica. Increasing values of A_2 reflect better dispersion. Negative A_2 indicates an immiscible system where the intensity rises at lowest-q. reflecting the formation of a new macro-phase at large scales.

The accumulated strain in a filled elastomer is proportional to the residence time in the mixer [8,24]. For a staged mixing process, the mean accumulated strain, γ_{acc} will approximately be a weighted sum of the accumulated strain, γ_{acc} for the mixing stages, j.

$$\gamma_{acc} = N\Psi \sum_{j=1}^{\alpha} (t_f - t_{add,j})\Big/_{\alpha} \quad (5)$$

where, Ψ is a function of system parameters e.g. mixer geometry, N is the revolutions per minute of the mixing rotors or the shear rate, t_f is the time at which the nanocomposite was discharged, and $t_{add,j}$ indicates the time of addition of equal quantities of filler. For studies conducted on the same mixer without any alteration to rotor geometry, Ψ is a constant. Equation (5) assumes that the total volume of the compound being mixed in the chamber remains constant throughout the entire mixing procedure [25]. Equation (5) also assumes constant temperature in the mixer since it assumes constant viscosity. While the system might be normalized by the RPM and temperature, the mixer constant (or some variant) would technically not be constant for each case. These issues will be explored in follow-up experiments and are noted here for clarification.

For a thermally dispersed colloidal system, dispersion is governed by fluctuations in concentration, which are countered by the osmotic compressibility. In kinetically dispersed nanocomposites, accumulated strain might play a similar role to temperature in equilibrated systems. Larger strains lead to greater dispersion just as higher temperature leads to better dispersion. Since the average accumulated strain, γ_{acc}, is proportional to mixing time, an analogy to the van der Waals equation can be proposed substituting mixing time (accumulated strain) for temperature. In this colloidal analogy a van der Waals model [24] can be fit to the dispersion quantified by the second virial coefficient such that,

$$B_2 = A_2\left(M_{agg}^{\,2}\Big/_{N_A}\right) = b^* - a^*\Big/_{\gamma_{acc}} \quad (6)$$

where, b^* is related to the excluded volume of the dispersed aggregates and is expected to be a function of the type of filler [24]. a^* may be related to the interactions between filler and the polymer in the context of the mixing process. In this paper, an attempt has been made to quantify the extent of dispersion based on mean accumulated strain experienced by the filler particles under different number of mixing stages. Additionally, the morphological dependence of carbon black and flame synthesized carbon-coated silica fillers [26] on the proposed pseudo van der Waals constants, b^* and a^* was established. Kohls et al. [27] have shown that these carbon-coated fumed-silica powders display enhanced elastomer reinforcement compared to uncoated fumed silica.

2. Experimental

The filled elastomers were mixed in a 50g Brabender mixer at a rotor speed of $N = 60$ RPM for $t_f = 20$ min. The temperature at the start of mixing was 121 °C (250 °F). The air-cooled mixing chamber's temperature was maintained at 130 °C (266 °F) during the mixing process. For this study, commercial polybutadiene rubber, BR45 (45 indicating Mooney Viscosity) with a density of 0.9 g cm^{-3} was used. Additionally, the antioxidant, (N-(1,3-dimethylbutyl)-N′-phenyl-1,4-phenylenediamine) was used during the compounding process, as provided by TCI America. The fillers used in this study were commercially available Vulcan 8 (CB110) by Cabot that conforms to ASTM N110 target values, and flame synthesized fumed silicas coated with 0.5 wt% (0.5C–SiO_2), 0.8 wt% (1C–SiO_2) and 1.7 wt% (2C–SiO_2) carbon [26,28]. The densities of carbon black and fumed silica were 1.9 g cm^{-3} and 2.2 g cm^{-3} respectively.

Samples were prepared with filler concentrations of 0, 1 (dilute), and 50 phr (semi-dilute) where phr indicates parts per hundred of rubber. 1 phr is filer corresponds to about 1 wt% (~0.5 vol%) and 50 phr to about 33 wt% (~17 vol%). Initially the elastomer was charged to the mixer. The antioxidant was added once the temperature had reached 130 °C (266 °F). Following this the clock was started, and filler was charged based on the staged mixing schedule discussed below. For one stage (i.e. $\alpha = 1$), the entire quantity of filler was added at the beginning of the mixing process i.e. $t_{add,1} = 0$ min and the compound discharged at $t_f = 20$ mins. For two stages ($\alpha = 2$), one half of the filler quantity was added at the beginning of the mixing process such that $t_{add,1} = 0$ min, and the other half halfway through the mixing process such that $t_{add,2} = 10$ mins. This pattern was followed up to five stages. The average accumulated strain as normalized by the mixer geometry constant, Ψ, is listed in Table 1. Based on equation (5), the accumulated strain for a two-staged mixing process will be 75% of the single-staged process since half of the mixture resided for 100% while the other half resided for 50% of the mixing duration.

Table 1
Average accumulated strain for different mixing stages.

Number of Stages	1	2	3	4	5
Average Accumulated Strain $\gamma_{acc}{}^{\alpha}$	1200	900	800	750	720

[α]from equation (5) after normalizing with Ψ.

Samples for the scattering experiments were pressed between platens with a low compressive pressure ~2 psig and heated in an oven at 100 °C for 10 min. Small angle X-ray scattering measurements were performed at the 9-ID-C beamline at the Advanced Photon Source, Argonne National Laboratory, IL, USA on the USAXS/SAXS/WAXS instrument designed and operated by Dr. Jan Ilavsky [29].

Transmission electron micrographs were obtained by cutting ~80 nm sections with a cryo-ultramicrotome below the glass transition temperature of filled elastomer specimens and subsequently imaged on a TEM with an accelerating voltage of 25 kV and an emission current of 10 μA.

3. Results

Fig. 1 shows the scattering curve from a dilute (1phr) filler concentration for BR45-2C–SiO_2 processed through two stage mixing. At the lowest q, $0.0001 < q < 0.0004$ Å^{-1}, a power-law of about −3 slope is observed which may reflect micron-scale agglomerates [17]. At intermediate q, $0.003 < q < 0.008$ Å^{-1}, a power-law of d_f = -2.2 is observed for the mass fractal aggregates. Below the mass fractal regime in q, a Guinier knee is observed reflecting the radius of gyration of the aggregates. At high q, $0.015 < q < 0.04$ Å^{-1}, Porod scattering is observed with a power law slope of -4 indicating surface scattering from the smooth, sharp interface of the silica cores (primary particles).

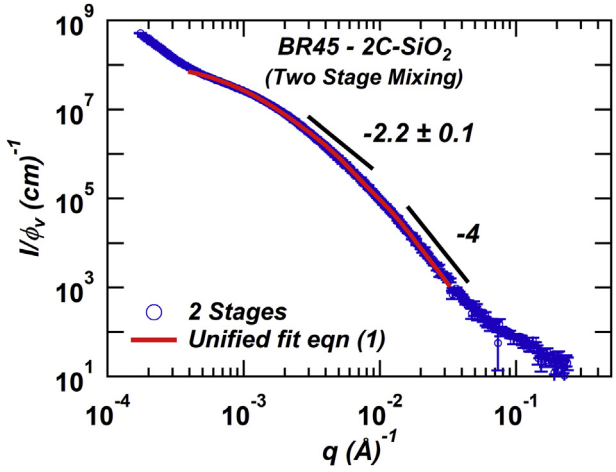

Fig. 1. Log-log plot of normalized intensity, $I(q)/\phi_V$, versus scattering vector, q, for dilute (1phr) 2C–SiO2 in BR45 processed under two stage mixing. The intermediate and low q regions were fit using the Unified Function given by equations (1) and (2). The power law slope of −4 is associated with surface scattering from primary particles whereas the slope of −2.2 ± 0.1 is for scattering from aggregates with d_f= 2.2.

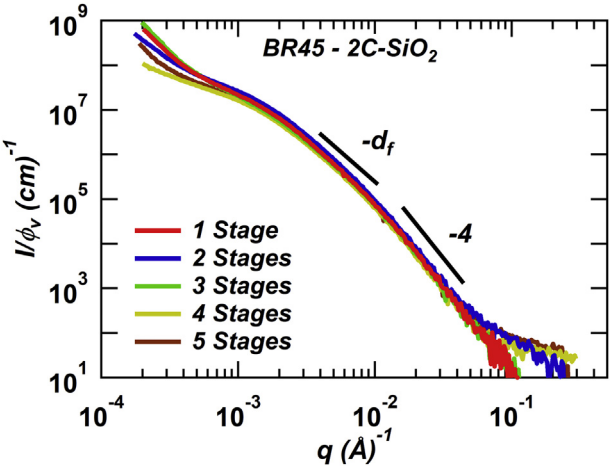

Fig. 2. Log-log plot of normalized intensity, $I(q)/\phi_v$, versus scattering vector, q, for dilute (1phr) concentration of 2C–SiO_2 in the BR45 elastomer matrix processed under distinct stages of filler addition. The curves superimpose well.

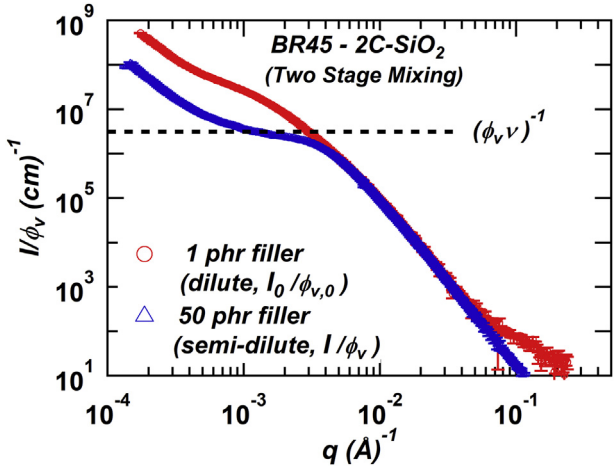

Fig. 3. Log-log plot of normalized intensity, $I(q)/\phi_V$, versus scattering vector, q, under dilute (1phr) and concentrated (50phr) filler concentrations of 2C–SiO2 in BR45 made by two stage mixing. The drop in normalized intensity is used to determine the screening parameter, ν from equation (3). The value of $(\phi_V \nu)^{-1}$ from the plot is 3. 2×10^6 from which $\phi_V \nu$ can be obtained. Dividing $\phi_V \nu$ by the volume fraction for 50phr filler (ϕ_V~0.17), results in $\nu \sim 1.8 \times 10^{-6}$ cm.

Between the mass fractal and Porod regimes a Guinier transition knee reflects the radius of gyration of the primary particles. The ratio of G_2 for the aggregates and G_1 for the primary particles added by 1 yields the weight average degree of aggregation which is about 90 primary particles/aggregate in this case.

As previously discussed, the regions of interest are the low and intermediate q regions in Fig. 1, $0.015 < q < 0.03$ Å^{-1}. The Unified Function given by equations (1) and (2) was used to fit the dilute scattering data and extract various morphological parameters in these two regions.

Fig. 2 shows the dilute filler concentration plots for BR45-2C–SiO_2 samples processed through the different mixing stages. For these samples, $\nu\phi_V$, in equation (3), is much smaller than $I(q,\phi_{V,0})/\phi_{V,0}$ at low concentrations and low q so that the observed intensity is not impacted by ν. For this concentration the entire filler structure can be measured. From Fig. 2, it is observed that with change in mixing procedure the scattering patterns are similar in the region of interest, $0.015 < q < 0.03$ Å^{-1}, indicating that on average, the filler aggregate structure does not change with different stages of mixing. The structural parameters obtained from the Unified Fit for all filler elastomer combinations can be found in the supplemental materials.

Fig. 3 shows the normalized intensity plots for dilute (1phr), $I_0(q,\phi_{V,0})/\phi_{V,0}$, and semi-dilute (50phr), $I(q,\phi_V)/\phi_V$ specimens of BR45-2C–SiO_2 processed through two-stage mixing. The high-q regions superimpose well. However, a significant drop in the normalized scattering intensity is observed in the intermediate-q region for the 50 phr sample. This normalized intensity loss, $(\nu\phi_V)^{-1}$ is used to compute the screening parameter, ν from equation (3). The loss in normalized intensity indicates that the larger structural features are screened out and an analysis, like the one for dilute curves via the Unified Function is not possible. Under semi-dilute conditions a local network emerges which is characterized by a mesh size [7,17–19].

For each specimen, the scattering intensity curves at three separate locations were analyzed yielding an average value of the screening parameter, ν. The values of ν for different elastomer-filler combinations are listed in Table 2. Other structural parameters relevant to this discussion such as the Sauter mean diameter, the diameter for a sphere with the same specific surface area as the primary particle, d_p, and the degree of aggregation, z can be computed from the fit parameters listed in Table S1 in the supplementary material [17]. These key morphological parameters along with the aggregate end-to-end distance, $R_{eted} = d_p z^{1/d_f}$, where $d_f = -P_2$ are also listed in Table 2. $\Delta\rho^2$ was 5.94×10^{21} cm^{-4} and 10.8×10^{21} cm^{-4} for carbon black and silica samples respectively.

Table 2
Calculated structural parameters from fit parameters to dilute (1phr) scattering curves listed in Table S1 in the Supplementary material; screening parameter, ν from equation (3), resulting from loss in scattering intensity from semi-dilute (50 phr) samples for all elastomer-filler combinations.

BR45 - Filler	*Number of stages*	*Dilute (1 phr)*			*Semi-dilute (50 phr)*
		d_p	z	R_{eted}	ν ($\times 10^{-6}$ cm)
2C–SiO_2	1	29 ± 2	95 ± 10	210 ± 30	2.2 ± 0.3
	2	29 ± 1	92 ± 10	220 ± 20	1.8 ± 0.3
	3	29 ± 3	90 ± 10	210 ± 30	1.7 ± 0.3
	4	29 ± 1	82 ± 10	210 ± 20	1.7 ± 0.3
	5	30 ± 1	79 ± 4	200 ± 4	1.3 ± 0.09
1C–SiO_2	1	13 ± 0.6	640 ± 70	150 ± 12	4 ± 1
	2	14 ± 0.3	580 ± 20	143 ± 7	3.8 ± 0.9
	3	14 ± 0.5	630 ± 80	151 ± 7	3.7 ± 0.1
	4	14 ± 0.4	600 ± 30	143 ± 5	3.6 ± 0.3
	5	13 ± 0.3	660 ± 20	147 ± 4	3.2 ± 0.2
0.5C–SiO_2	1	15 ± 0.5	340 ± 40	121 ± 3	4.7 ± 0.5
	2	15 ± 0.3	340 ± 20	120 ± 2	3.5 ± 0.4
	3	16 ± 0.4	250 ± 30	118 ± 1	4 ± 1
	4	16 ± 1	280 ± 50	127 ± 2	3.9 ± 0.2
	5	17 ± 0.3	240 ± 10	119 ± 2	3.7 ± 0.5
CB110	1	28 ± 1	23 ± 3	110 ± 10	16 ± 1
	2	28 ± 2	26 ± 5	120 ± 20	14 ± 3
	3	28 ± 1	27 ± 0.4	130 ± 30	15 ± 2
	4	28 ± 1	27 ± 4	130 ± 10	12 ± 1
	5	28 ± 0.4	29 ± 4	140 ± 20	12 ± 1

Fig. 4 shows transmission electron micrographs for 2C–SiO_2 filler dispersed in polybutadiene. For 2C–SiO_2, d_p is about 30 nm and the aggregate end to end distance is on the order of 200 nm. Owing to the limited resolution of the image in Fig. 4(a), the size of the primary particle cannot be discerned, however, the aggregate size is about a third of the entire scale bar and seems consistent with the USAXS results in Table 2. The micrographs help to illustrate the effects of structural screening within the compounds themselves. In Fig. 4(a) the features of the aggregate are clearly discernable. However, as the concentration of these fillers increase in Fig. 4(b) the size of the aggregates and details of the branching of the aggregates become more difficult to view. In Fig. 4(a)–insets, simulated aggregates based on the scattering fit parameters using Mulderig's diffusion limited aggregation program are shown for comparison [30]. This shows a favorable direct comparison

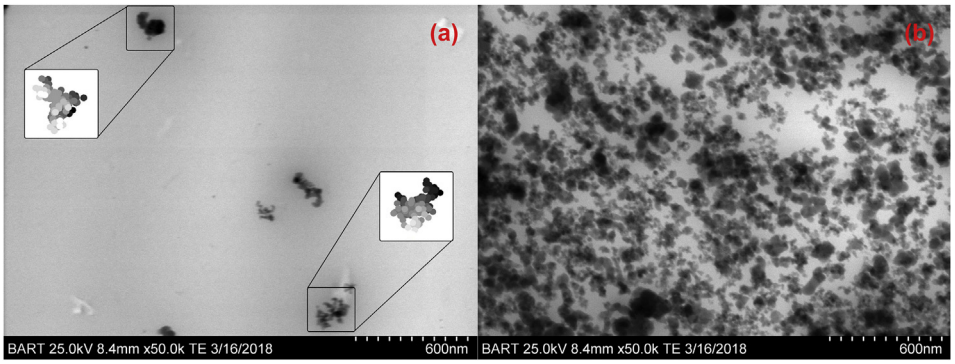

Fig. 4. Transmission electron micrographs of the compounds filled with 2C–SiO_2 dispersed in polybutadiene BR45; (a) 1 phr of silica, (b) 50 phr of carbon-coated fumed silica. The full range of each scale bar is 600 nm. (a)-inset 2C–SiO_2 aggregate created using the USAXS fit parameters [30]. A screening length of about 200 nm is possible in (b) as the space between aggregates.

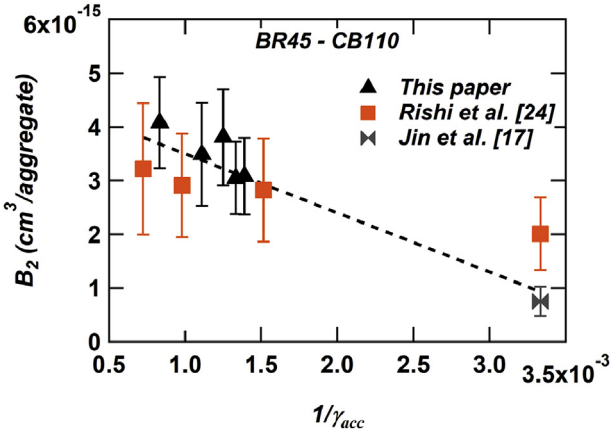

Fig. 5. A plot reflecting the relationship between the pseudo-second virial coefficient (B_2) and inverse accumulated strain modelled through equation (6) for BR45-CB110 samples processed under different conditions (triangles for this paper, squares for reference [24] and bowtie for reference [17]). The applicability of the model is tested against other reported values of the same nanocomposite. The dashed line shows a linear dependence between B_2 as a function of inverse accumulated strain modelled over the three sets of data points (triangles, squares and bowtie).

of scattering and microscopy.

A_2 was calculated from equation (4) and the parameter (ν) listed in Table 2, whereas B_2 was calculated using equation (6). Wang et al. showed that the single step mixing procedure is better than the conventional multistep process [10]. In fact, for two stage mixing, a larger amount of filler addition in the initial stage yielded better results, as reported by Hasan et al. [9]. However, no significant difference in mechanical properties was reported by Choi et al. [31].

Fig. 5 shows B_2 as a function of the inverse average accumulated strain following equation (6). Literature data [17,24] was used to compare with the staged mixing data in this article for the same filler-elastomer combination, i.e. BR45-CB110, with fairly consistent results. The dashed line in Fig. 5 is the error weighted fit to three sets of data points (black triangles, orange squares and grey bowties) and shows the feasibility of the proposed colloidal model. Note that the reported values [17,24] of the pseudo second virial coefficient, A_2, were scaled to B_2 using the average degree of aggregation, $z = 26 \pm 3$ from Table 2 for BR45–CB110 nanocomposite. The result in Fig. 5 indicates that aggregate dispersion as modelled using accumulated strain in equation (6) can be applied to other processing conditions such as varying mixing time and perhaps varying shear rates if the mixing geometry remains unchanged.

In Fig. 6, B_2 varies linearly with inverse average accumulated strain. It can be seen that B_2 increases with increasing accumulated strain for all of the specimens studied. B_2 is generally greater for carbon-coated silicas (refer left ordinate axis) as compared with carbon black (refer

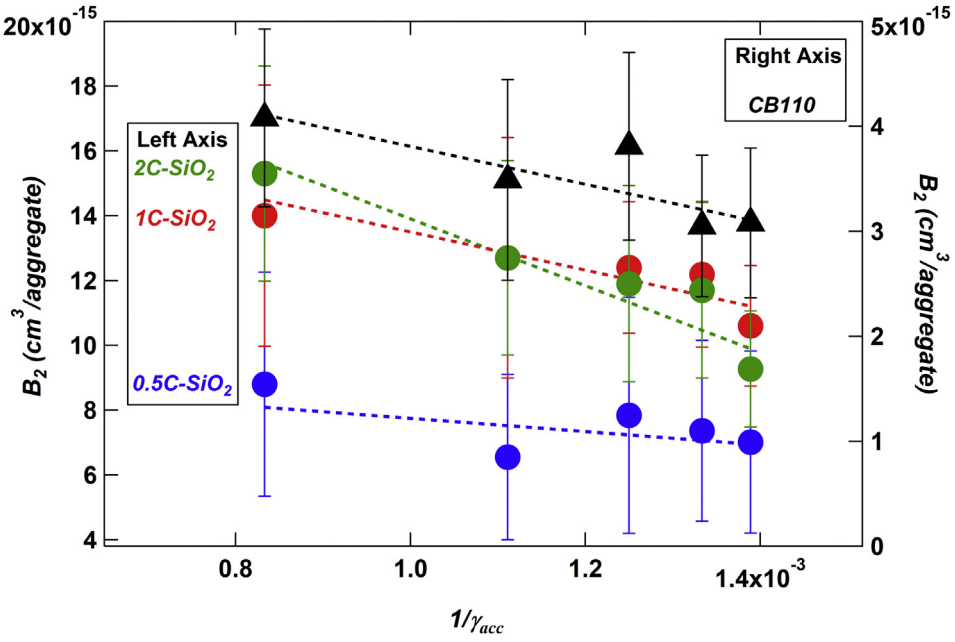

Fig. 6. A plot reflecting the van der Waals model for accumulated strain dependence drawing an analogy between effect of temperature for colloids and accumulated strain for nanocomposites. All three carbon-coated silicas (refer left axis) indicated by solid circles seem to disperse better than the carbon black (refer right axis) indicated by solid triangles. Fits to the data are indicated by dashed lines per equation (6).

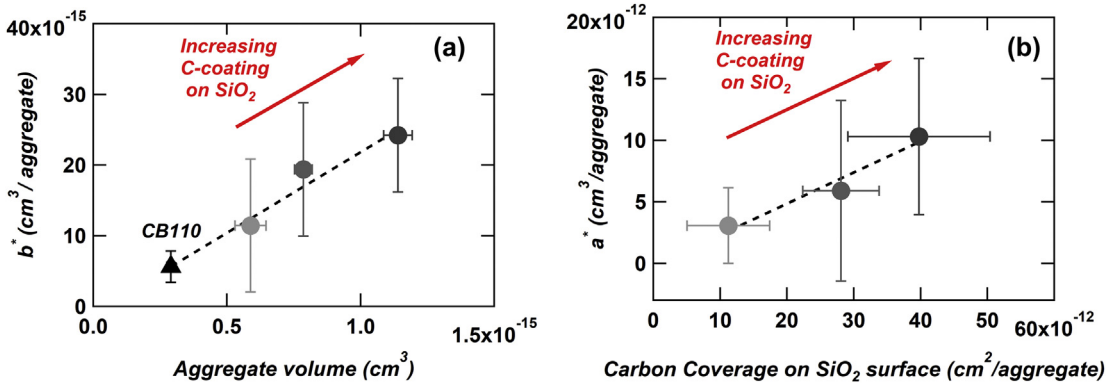

Fig. 7. (a) A plot depicting the pseudo-excluded volume, b^*, as a function of aggregate volume extrapolated from B_2 vs. inverse accumulated at infinite strain in Fig. 6; (b) A plot showing the dependence of pseudo-interaction parameter, a^*, as a function of surface coverage of carbon coated on silica.

right ordinate axis) which means that carbon-coated silicas disperse better than carbon black. This could be attributed to the larger aggregate size (R_{eted}) of the carbon-coated silicas as listed in Table 2. Larger aggregates will display a larger lever arm in the same shear force field and consequently disperse better. Additionally, carbon-coated silicas with a larger degree of aggregation (1C–SiO_2) disperse better as opposed to aggregates with lower z (0.5C–SiO_2) even though the size of their primary particles (d_p) is comparable within the experimental error.

The lines in Fig. 6 can be extrapolated to infinite accumulated strain yielding b^* which represents the average excluded volume of the filler aggregates [24]. Low accumulated strain occurs at shorter residence times or by breaking the mixing cycle into a substantial number of stages. In such a situation, incomplete wetting of the filler particles by the elastomer is expected so that B_2 approaches 0. This pseudo-Boyle point is calculated as $\gamma_{acc}{}^* = {}^{a^*}/_{b^*}$, and represents the critical accumulated strain for dispersion or the wetting time at constant strain rate.

Fig. 7(a) shows a plot of pseudo-excluded volume, b^* as a function of aggregate volume ($V_{agg} = z\pi {d_p}^3/6$) determined from the parameters in Table 2. A linear trend is observed as expected. Based on the hard sphere model, the excluded volume is expected to be 4 times the particle volume. However, this trend is not expected for fractal filler aggregates. The fit in Fig. 7(a) indicates a slope of ~20 which is not unrealistic considering the aggregate anisotropy.

Fig. 7(b) shows a plot of a^* as a function of carbon coverage on the fumed-silica surface. This pseudo-interaction parameter representing filler attraction was shown to be a function of matrix viscosity [24] and is expected to be constant since the same matrix elastomer was used for compounding the fillers. However, a linear trend with increasing carbon coverage on the silica surface indicates an increase in filler attraction. This is possible since an increase in carbon content on the surface could effectively shield the silica core-core repulsions.

The ratio of $\frac{a^*}{b^*}$ i.e. the critical accumulated strain and the filler wetting time varies with carbon coating because the structure for the silica also varies significantly with carbon coating. The van der Waals approach allows for the separation of the structural effect from the interfacial effect and yields a design toolbox to improve dispersion in these kinetically dispersed nanocomposites.

4. Conclusions

Compounding of nanofillers in elastomers involves surface wetting, agglomerate breakup and dispersion of aggregate particles in a complex rheological environment. Several general rules can be applied to these mixing operations. In this paper it was considered that the dispersion of aggregates should be related to the accumulated strain in a milling operation. The accumulated strain is proportional to the mean residence time under the assumption of a constant mixing volume. This was demonstrated for four fillers using a new measure of filler nano dispersion based on a colloidal model using the van der Waals equation and small angle X-ray scattering. For these fillers it was demonstrated that there is a reduced dispersion for staged mixing operations that was consistent with the van der Waals model for the pseudo-virial coefficient. For these compounds the best dispersion occurs in a single mixing stage where the maximum accumulated strain occurs. The effect of mixing time in staged mixing [24] on filler dispersion has been evaluated ignoring the details of filler distribution in the mixer. Future work will explore the effects of fill factor [25] on dispersion as well as the impact of mixing temperature, and rotor speed.

Notes

The authors declare no competing financial interest.

Acknowledgements

This work was supported by the National Science Foundation through grants CMMI-1635865 and CMMI-1636036. Alex McGlasson and Michael Chauby were supported by a Research Experience for Undergraduates supplemental grant CMMI-1761420 associated with CMMI-1635865. Use of the APS, an Office of Science User Facility operated for the U.S. Department of Energy (DOE) Office of Science by Argonne National Laboratory, was supported by the U.S. DOE under contract no. DE-AC02-06CH11357. The USAXS data were collected at the APS on the beamline 9-ID-C operated by the X-ray Science Division. We gratefully acknowledge the vital assistance of Jan Ilavsky and his staff at 9-ID-C.

Appendix A. Supplementary data

Supplementary data to this article can be found online at https://doi.org/10.1016/j.polymer.2019.121765.

References

[1] G.R. Cotten, Mixing of carbon black with rubber: IV. Effect of carbon black characteristics, Plast. Rubber Process. Appl. 7 (1987) 173–178, https://doi.org/10.1007/s13233-014-2119-5.
[2] A.Y. Coran, J.-B. Donnet, The dispersion of carbon black in rubber Part I. Rapid method for assessing quality of dispersion, Rubber Chem. Technol. 65 (1992) 973–997, https://doi.org/10.5254/1.3538655.
[3] A.Y. Coran, J. Donnet, The dispersion of carbon black in rubber Part II. The kinetics of dispersion in natural rubber, Rubber Chem. Technol. 65 (1992) 998–1015, https://doi.org/10.5254/1.3538656.
[4] F. Bohin, D.L. Feke, I. Manas-Zloczower, Analysis of power requirements and dispersion quality in batch compounding using a dispersion model for single agglomerates, Rubber Chem. Technol. 69 (1996) 1–7, https://doi.org/10.5254/1.3538355.
[5] D.M. Kalyon, S. Aktaş, Factors affecting the rheology and processability of highly

filled suspensions, Annu. Rev. Chem. Biomol. Eng. 5 (2014) 229–254, https://doi.org/10.1146/annurev-chembioeng-060713-040211.
[6] M.M. Rueda, M. Auscher, R. Fulchiron, T. Périé, G. Martin, P. Sonntag, P. Cassagnau, Rheology and applications of highly filled polymers: a review of current understanding, Prog. Polym. Sci. 66 (2017) 22–53, https://doi.org/10.1016/j.progpolymsci.2016.12.007.
[7] K. Rishi, G. Beaucage, V. Kuppa, A. Mulderig, V. Narayanan, A. McGlasson, M. Rackaitis, J. Ilavsky, Impact of an emergent hierarchical filler network on nanocomposite dynamics, Macromolecules 51 (2018) 7893–7904, https://doi.org/10.1021/acs.macromol.8b01510.
[8] Z. Tadmor, C.G. Gogos, Principles of Polymer Processing, second ed., John Wiley & Sons, Inc., Hoboken, NJ, USA, 2006.
[9] A. Hasan, Rochmadi, H. Sulistyo, S. Honggokusumo, Effect of rubber mixing sequence variation upon bound rubber formation and its physical properties, Asian J. Chem. 25 (2013) 5203–5207.
[10] C.S. Wang, G.Z. Song, S.H. Zhao, N. Ren, D. Wang, Comparative study of the low-temperature single step mixing and multi-stage process mixing, Key Eng. Mater. 561 (2013) 113–118 https://10.4028/www.scientific.net/KEM.561.113.
[11] G. Geuskens, J.L. Gielens, D. Geshef, R. Deltour, The electrical conductivity of polymer blends filled with carbon-black, Eur. Polym. J. 23 (1987) 993–995, https://doi.org/10.1016/0014-3057(87)90047-4.
[12] J. Zhong, A.I. Isayev, X. Zhang, Ultrasonic twin screw compounding of polypropylene with carbon nanotubes, graphene nanoplates and carbon black, Eur. Polym. J. 80 (2016) 16–39, https://doi.org/10.1016/j.eurpolymj.2016.04.028.
[13] H. Tang, X. Chen, Y. Luo, Electrical and dynamic mechanical behavior of carbon black filled polymer composites, Eur. Polym. J. 32 (1996) 963–966, https://doi.org/10.1016/0014-3057(96)00026-2.
[14] X. Fu, J. Wang, J. Ding, H. Wu, Y. Dong, Y. Fu, Quantitative evaluation of carbon nanotube dispersion through scanning electron microscopy images, Compos. Sci. Technol. 87 (2013) 170–173, https://doi.org/10.1016/j.compscitech.2013.08.014.
[15] D.M. Kalyon, D. Dalwadi, M. Erol, E. Birinci, C. Tsenoglu, Rheological behavior of concentrated suspensions as affected by the dynamics of the mixing process, Rheol. Acta 45 (2006) 641–658, https://doi.org/10.1007/s00397-005-0022-x.
[16] D.M. Kalyon, A. Lawal, R. Yazici, P. Yaras, S. Railkar, Mathematical modeling and experimental studies of twin-screw extrusion of filled polymers, Polym. Eng. Sci. 39 (1999) 1139–1151, https://doi.org/10.1002/pen.11501.
[17] Y. Jin, G. Beaucage, K. Vogtt, H. Jiang, V. Kuppa, J. Kim, J. Ilavsky, M. Rackaitis, A. Mulderig, K. Rishi, V. Narayanan, A pseudo-thermodynamic description of dispersion for nanocomposites, Polymer 129 (2017) 32–43, https://doi.org/10.1016/j.polymer.2017.09.040.
[18] A. Mulderig, G. Beaucage, K. Vogtt, H. Jiang, Y. Jin, L. Clapp, D.C. Henderson, Structural emergence in particle dispersions, Langmuir 33 (2017) 14029–14037, https://doi.org/10.1021/acs.langmuir.7b03033.
[19] K. Vogtt, G. Beaucage, M. Weaver, H. Jiang, Thermodynamic stability of worm-like micelle solutions, Soft Matter 13 (2017) 6068–6078, https://doi.org/10.1039/C7SM01132F.
[20] G. Beaucage, Approximations leading to a unified exponential/power-law approach to small-angle scattering, J. Appl. Crystallogr. 28 (1995) 717–728, https://doi.org/10.1107/S0021889895005292.
[21] G. Beaucage, Determination of branch fraction and minimum dimension of mass-fractal aggregates, Phys. Rev. E. 70 (2004) 031401, , https://doi.org/10.1103/PhysRevE.70.031401.
[22] G. Beaucage, H.K. Kammler, S.E. Pratsinis, Particle size distributions from small-angle scattering using global scattering functions, J. Appl. Crystallogr. 37 (2004) 523–535, https://doi.org/10.1107/S0021889804008969.
[23] J.S. Pedersen, C. Sommer, Temperature dependence of the virial coefficients and the chi parameter in semi-dilute solutions of PEG, Scatt. Methods Prop. Polym. Mater, Springer Berlin Heidelberg, Berlin, Heidelberg, 2005, pp. 70–78, , https://doi.org/10.1007/b107350.
[24] K. Rishi, V. Narayanan, G. Beaucage, A. McGlasson, V. Kuppa, J. Ilavsky, M. Rackaitis, A thermal model to describe kinetic dispersion in rubber nanocomposites: the effect of mixing time on dispersion, Polymer 175 (2019) 272–282, https://doi.org/10.1016/j.polymer.2019.03.044.
[25] D. Kim, J.S. Lee, C.M.F. Barry, J.L. Mead, Effect of fill factor and validation of characterizing the degree of mixing in polymer nanocomposites, Polym. Eng. Sci. 47 (2007) 2049–2056, https://doi.org/10.1002/pen.20920.
[26] H.K. Kammler, S.E. Pratsinis, Electrically-assisted flame aerosol synthesis of fumed silica at high production rates, Chem. Eng. Process. Process Intensif. 39 (2000) 219–227, https://doi.org/10.1016/S0255-2701(99)00082-3.
[27] D. Kohls, G. Beaucage, S.E. Pratsinis, H. Kammler, G. Skillas, Carbon coated silica for elastomer reinforcement, MRS Proc. 661 (2000), https://doi.org/10.1557/PROC-661-KK9.4 KK9.4.
[28] H.K. Kammler, R. Mueller, O. Senn, S.E. Pratsinis, Synthesis of silica-carbon particles in a turbulent H2-air flame aerosol reactor, AIChE J. 47 (2001) 1533–1543, https://doi.org/10.1002/aic.690470707.
[29] J. Ilavsky, P.R. Jemian, A.J. Allen, F. Zhang, L.E. Levine, G.G. Long, Ultra-small-angle X-ray scattering at the advanced Photon Source, J. Appl. Crystallogr. 42 (2009) 469–479, https://doi.org/10.1107/S0021889809008802.
[30] A. Mulderig, G. Beaucage, K. Vogtt, H. Jiang, V. Kuppa, Quantification of branching in fumed silica, J. Aerosol Sci. 109 (2017) 28–37, https://doi.org/10.1016/j.jaerosci.2017.04.001.
[31] S.-S. Choi, Influence of mixing procedure on properties of silica filled epoxidised natural rubber compounds, Korea Polym. J. 8 (2000) 192–198.